IEEE Access
Multidisciplinary ⋮ Rapid Review ⋮ Open Access Journal

Received February 15, 2021, accepted March 16, 2021, date of publication March 19, 2021, date of current version March 29, 2021.

Digital Object Identifier 10.1109/ACCESS.2021.3067312

Batteryless and Self-Reconfigurable Multimode RF Network using All-Passive Energy Smart-Sensing

DUC ANH PHAM, RATANAK PHON, YEONJU KIM, AND SUNGJOON LIM, (Member, IEEE)
School of Electrical and Electronics Engineering, Chung-Ang University, Seoul 06974, Republic of Korea

Corresponding author: Sungjoon Lim (sungjoon@cau.ac.kr)

This work was supported by the National Research Foundation of Korea (NRF) Grant funded by the Ministry of Science and ICT (MSIT), Korea Government under Grant 2021R1A2C3005239 and Grant 2021R1A4A2001316.

ABSTRACT In recent years, replacing the external control stimuli with internal control using characteristics of radio frequency (RF) signals (such as waveform or power level) has attracted considerable attention to the design of reconfigurable multifunctional RF devices. However, even with the most exciting techniques, the control process always needs a chip-based system to sense the power level or waveform of the incident RF signal, which is realised by additional supporting electronic components of the sensing and microcontroller circuits. Therefore, to achieve a batteryless structure, a majority of conventional works focus on using energy harvesters to convert energy from external environmental sources to DC energy for the electronic circuits. Herein, we propose a novel alternative approach to replace the traditional energy harvesters in batteryless RF devices with all-passive energy smart-sensing circuits. By exploiting the features of a nonlinear semiconductor device under different incident RF power values, the proposed network can passively self-sense the RF power level and dynamically self-control RF signal flow and power ratio. The operation of the proposed network can be considered as purely self-adaptation with control from the RF power level. Moreover, normal RF devices can be transformed to all-passive and batteryless purely self-reconfigurable devices via integration with the proposed structure. As proof of concept, the proposed network is integrated with a two-port antenna to experimentally demonstrate its purely self-reconfigurable polarisation. The proposed strategy is hereby expected to extend the field of batteryless self-reconfigurable multifunctional RF devices and pave promising new paths for the development of future intelligent, smart RF devices.

INDEX TERMS Self-reconfigurable, self-adaption, batteryless, multifunctional, all-passive, energy smart-sensing.

I. INTRODUCTION

Since the invention of the first practical radio frequency (RF) system by Guglielmo Marconi [1], [2] in the 1890s, the field of wireless communication has experienced significant diversity with more than a century of intense study and rapid development. From the beginning, controlling radio frequency (RF) signal flow and ratio has always been an important roles for the design of both RF devices and systems. For instance, the RF signal flows in the transmitting (TX) and receiving (RX) directions must be separated when the RF transmitter and receiver share a single antenna [3]–[5]. Moreover, channelisation for frequency division is mandatory in systems that use multiple modulation methods and carriers with single radiated component because of the simultaneous existence of several frequencies [6]. Furthermore, the RF signal flow directly affects the behaviours of modern RF systems such as the multiple input multiple output (MIMO) system [7], [8], and RF devices such as multi-feed antennas [9], [10], phase shifters [11], [12], metasurfaces [13]–[16], and so on. In contrast, excess RF power in one part of an RF system can permanently damage or interfere with the other parts [17], [18]. From the broader system-level view, a typical wireless system contains multiple wireless base stations (BSs) that use similar frequencies [19], [20]; the output RF power ratio between these BSs must therefore be

The associate editor coordinating the review of this manuscript and approving it for publication was Tutku Karacolak.

considered to achieve reasonable carrier-to-noise ratios. The power ratios between different branches of signal flows are also crucial to the behaviour of an RF device, such as the polarisation of a dual-feed antenna [21]–[23], or the beam direction of an antenna array [24]–[27]. Based on these observations, it is obvious that controlling the RF signal flow and power ratio is important and indispensable to determine the behaviour of an RF device.

Conventionally, the strategies for tailoring RF signal flows and ratios can be divided into two groups: static and dynamic manipulations. Static manipulation refers to techniques whose processes are fixed and cannot be reconfigured [28]–[31]. In contrast, dynamic manipulation refers to techniques whose processes can be reconfigured and controlled. Owing to their flexibility and adaptability, dynamic manipulation methods are more suitable for modern intelligent wireless systems. RF signal flows can be dynamically controlled using switch components, such as the single-pole double-throw (SPDT) switch, single-pole multiple-throw switch, double-pole double-throw (DPDT) switch [32]–[35], positive-intrinsic-negative (PIN) diode [36]–[40], transistor [41]–[43], or RF microelectromechanical system (MEMS) [44], [45]. On the other hand, the RF power ratio can be conventionally handled with a variable gain amplifier and an attenuator. Generally, both RF signal flow and power ratio manipulations require external control stimuli along with additional supporting electronic components, such as a microcontroller circuit and DC power supply.

In the era of modern, intelligent wireless systems, the demand for self-operating or self-adapting devices has rapidly increased. To enable a typical reconfigurable RF device/system to be self-reconfigurable or self-adaptable, replacing the external control stimuli with internal control based on the characteristics of RF signals (waveform, frequency, and power level) [46]–[49] and eliminating RF device dependence on the power supply are two indispensable duties. However, most reported works have needed sensing devices to detect the internal characteristics of RF signals and microcontrollers to subsequently configure the state of the RF device/system. Batteryless electronic devices are typically achieved using energy harvesters [50] to convert the energy from an external environmental source (such as mechanical [51], piezoelectric [52], [53], and RF energy harvesting [54], [55]) into DC energy for the electronic circuits. In general, the traditional solutions for self-operating RF devices still require additional supporting electronic subcircuits and subsystems. Although self-operation can be achieved, the complexities of the devices and systems are significantly increased. Moreover, with the rapid development of wireless communication systems, requirements for higher data rates and lower latency connections have risen steeply, which have driven the development of millimetre-wave communication techniques [56]. When the operational frequency of a system is increased, creating control lines or sub-circuits becomes more challenging and places greater pressure on the main control system.

Accordingly, herein, we propose a novel batteryless multimode self-reconfigurable RF network to dynamically control the RF signal flow and ratio after RF power modulation. Further, a novel alternative approach of all-passive energy smart-sensing is presented to replace the traditional method and enable automatic self-switching batteryless operation between the multi-states of RF devices without the support of other electronic devices or DC power supply. The proposed strategy is primarily based on exploiting the characteristics of nonlinear semiconductor devices under different incident RF power values to passively self-sense the power level and integrate it with a static navigator to control the signal flow. We believe that the proposed strategy paves an extendable path for self-operating RF devices and systems as well as enables steady development of future smart RF devices and systems. Moreover, the proposed strategy can be extended to applications in the millimetre-wave frequency range, in which creating sub-circuits or subsystems have been challenging owing to the extremely short wavelengths. First, the operational mechanism of the proposed network is outlined, and the theoretical considerations are explained. Subsequently, we present the strategy to achieve a batteryless multimode self-reconfigurable RF network that can be dynamically controlled by RF power modulation without additional supporting electronic components. As proof of concept, using the proposed network, a purely self-polarisation-reconfigurable (PSPR) antenna, which can be configured by power modulation without any supporting electronic devices, is designed. The concept of ''purely self-reconfigurable'' is introduced to present devices whose reconfiguration mechanisms are controlled automatically and independently without external control signals, bias circuits, sensing circuits, or DC power supplies. Finally, the potential directions for application of the proposed work are discussed.

II. PRINCIPLE AND DESIGN

A. PROPOSED CONCEPT AND OPERATIONAL ILLUSTRATION

Fig. 1 illustrates the operational mechanism of the proposed network. The power dependence is achieved with the intrinsic characteristics of the proposed device instead of using sensing circuits or energy harvesters for the subsystem supply. Thus, the proposed network can passively self-sense the RF power level and dynamically self-control the RF signal flow and power ratio without using any detectors, sensors, microcontrollers, or power supplies; this novel feature makes the proposed design unique compared with other existing designs. The term ''all-passive energy smart-sensing'' is used to emphasize the novel features of the proposed network.

The RF signal tailoring processes of the proposed network can be considered as purely self-adaptive, in which each port is visualized as a water pipe with two separate

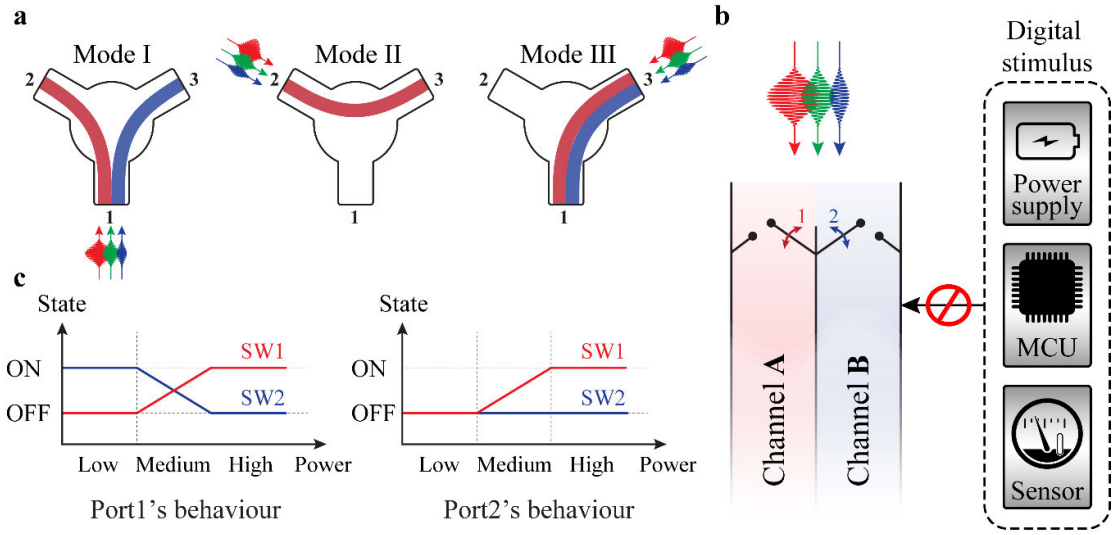

FIGURE 1. Operation mechanism of the proposed network. RF signal tailoring process is automatically controlled by RF power modulation without supporting electronic components or power supplies. The process can be considered as a purely self-adaption. (a) Different route configurations for channels A and B for each mode. (b) Illustration of port operation, where each channel has power-dependent inputs and can be described as switches that can block (when the switch is OFF) or allow (when the switch is ON) inputs to the channels. (c) Behaviours of ports with different input power values.

halves presented as channels A and B. Fig. 1(c) depicts the behaviours of port 1 and port 2 under different power levels. Specifically, when a low-power RF signal flows into port 1, channel A is blocked, whereas channel B is opened. Hence, the incident wave only follows the route of channel B.

In contrast, the high-power incident wave only follows the route of channel A. Furthermore, the medium-power incident wave places both switches in incomplete ON and OFF states, thereby allowing the incident wave to flow into both channels. When the low-power RF signal flows into port 2, both channels are blocked, which completely reflects the incident wave. When the power of the incident wave is increased, the switch of channel A starts opening whereas that of channel B remains in its OFF state. Hence, the medium-power incident wave is partly reflected and partly flows into channel A. The amount of the wave flowing into channel A increases with increment of the incident wave power until the switch for channel A is completely opened. Port 3 does not depend on the power levels of the incident signals; thus, the two switches are opened with any power level.

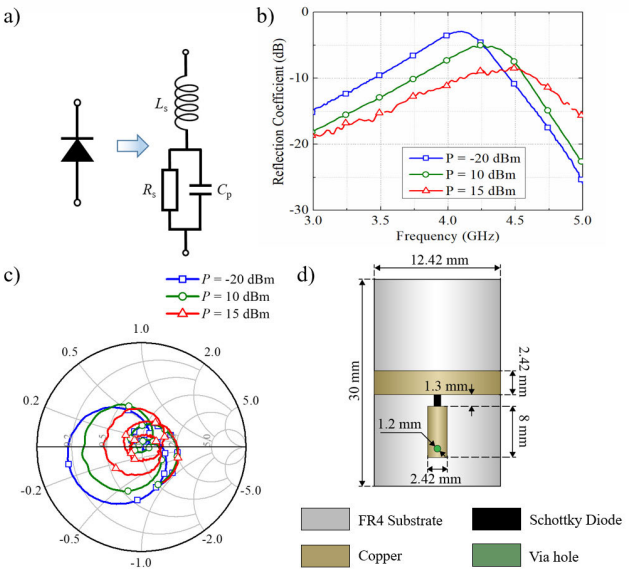

FIGURE 2. Proposed power-dependent network. (a) Equivalent circuit of a diode. (b) Input power level effects on the reflection coefficients and (c) input impedance. (d) Geometry dimensions of the proposed power-dependent network.

B. BATTERYLESS SELF-RECONFIGURABLE MULTIMODE RF NETWORK

Conventional RF devices and systems use diodes as controllable switches, with the two main states ON and OFF controlled by the bias voltages. However, a diode can also self-vary without using bias voltage, such as the power limiter in an RF receiver system. Although the input power does not place the diode in a complete ON state, the incident power level still affects the diode's equivalent values of series resistance R_s, series inductance L_s, and parallel capacitance C_p, which are demonstrated in Fig. 2(a). Hence, it is possible to design a purely passive two-port network that achieves impedance matching at a specific power level and mismatch at other power levels. The signal at the appropriate power level can be completely delivered through the network, whereas the signal at other power levels are partly or completely reflected. By placing the network under match/mismatch states, we can control both the RF signal flow and output power only by manipulating the input

TABLE 1. Schottky diode SMS7630 equivalent circuit values.

Input power (dBm)	L_s (nH)	C_p (pF)	Rp (Ω)
-20	1.5	0.22	5000
-10	1.4	0.215	4700
0	1.3	0.2	4500
10	1.2	0.19	2400
15	0.8	0.18	800

power levels. To the best of our knowledge, in high-frequency circuits and systems, there are no reported designs that exploit this feature to manipulate RF signal flow and power ratio. The power sensing mechanism can be considered as an all-passive smart-sensing scheme because there are no detectors, sensing circuits, or energy harvesters which have been used.

As a proof of principle, we initially designed and investigated an RF network using a Schottky diode SMS7630 (forward voltage $V_f = 135$–240 mV at 1 mA) to demonstrate mentioned power-dependent characteristics. Firstly, by conducting measurements and parametric studies with full-wave analysis, the diode's equivalent values of R_s, L_s, and C_p at different power levels were determined, as given in Table 1. A power-dependent network was then designed and fabricated with a 1.2 mm thick FR4 substrate with dielectric constant $\varepsilon = 4.1$ and loss tangent $\delta = 0.02$. The performance of the designed power-dependent network is measured with a Keysight N5227B PNA; input power levels from -20 to 15 dBm were investigated. As can be observed in Fig. 2(b) and (c), the changes on input power level are able to drive the designed network from impedance matching to mismatch state. Specifically, the measured input impedances at 4 GHz varies from 11.05–18.78j to 35.44–20.43j Ω with input power varies from -20 to 15 dBm. The geometry dimensions of this purely passive power-dependent network are given in Fig. 2(d).

Based on the aforementioned mechanism, the RF signals at different power levels are classified and routed in different directions, although the waves still traverse the same main route. To exploit these differences in signal flows, we propose a batteryless self-reconfigurable multimode (BSRM) network to dynamically control RF signal flow and ratio without additional supporting components (such as controller, sensing, DC power supply circuits), as depicted in Fig. 3. The proposed network is self-reconfigurable via control of incident RF power level. The equivalent circuit of proposed network is presented in Fig. 3(a), and the operational demonstration is depicted in Fig. 3(b)–(d). The circuit structure has the combined form of a power-dependent network and a static navigator. In our design, this structure was realised using a circulator operated along with a diode network at pin *C-2* of the internal circulator. The proposed structure uses a Schottky SMS7630 diode, represented by the combination of L_s, R_s, and C_p in the equivalent circuit. Meanwhile, C_{TL} and L_{TL} represent the inductance and capacitance of the transmission line that connects the internal circulator with the diode network. By configuring a power-dependent network at pin *C-2* of the internal circulator, the signal that flows from the outside into port 2 or from the internal circulator to the diode network can be manipulated in other directions only by controlling the RF power level.

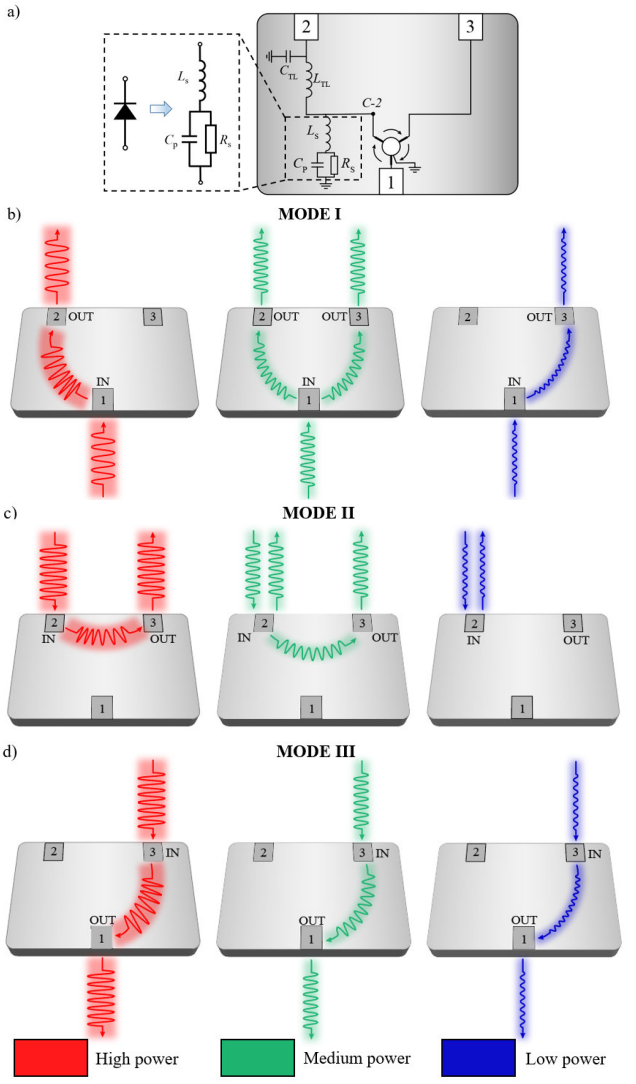

FIGURE 3. Proposed batteryless self-reconfigurable multimode (BSRM) network for dynamically controlling RF signal flows and ratios. (a) Equivalent circuit diagram. (b–d) Signal flows for high, medium, and low power signal levels in Mode I, Mode II, and Mode III, respectively.

The proposed network operates under three different modes, and the mode number represents the port number into which the signal flows. Each mode is further divided into three sub-states for high, medium, and low-power signals. For instance, state I-H represents the case where the incident high-power signal is delivered to port 1, whereas the low-power signal flowing into port 1 is represented by state I-L. The state of the proposed network can be manipulated

only by modulating the power level of the incident signal (Fig. 3(b)–(d)). In state I-H, the signal flows into port 1 and flows out at port 2. When the power level of the input signal is decreased to the low-power threshold, the proposed structure passively changes to state I-L. In this state, the signal flows into port 1 and flows out at port 3. Furthermore, with the medium input power level, designated as state I-M, one part of the RF signal flows out at port 2 and the remaining part flows out at port 3. In general, the proposed network at mode I functions as a controllable power divider manipulated by the RF power level. In state II-H, the high-power signal is delivered from port 2 to port 3. Passively manipulating the operational state to II-L by decreasing the signal level to low power allows the incident signal to be entirely reflected. With medium input power, designated as state II-M, the signal will be partly reflected and partly delivered to port 3. Generally, the proposed network at mode II functions as a filter that only allows signals with the appropriate power levels. Mode III does not depend on the power level, and the signal is delivered from port 3 to port 1 with any input power level.

The relationship of power at the three ports are considered to further explain the control mechanism of the proposed network based on the power ratio. Assume that T_{21}, T_{31}, and T_{32} are the transmission coefficients of the signal from port 1 to port 2, port 1 to port 3, and port 2 to port 3, respectively; Γ_2 is the reflection coefficient of the signal flowing into port 2; P_{low} and P_{high} are the sequentially low and high power thresholds of the designed BSRM network. Owing to the existence of the power-dependent network at output *C-2* of the internal circulator, T_{21}, T_{31}, T_{32}, and Γ_2 are functions of the input power $f\ (P_{in})$. Therefore, the relationship between the input and output signals in each state can be ideally expressed as a function of the input power using the following equations:

- Mode I:

$$P_1 = P_{in};$$

$$P_{out\_2} = P_{in} - |T_{21}| = \begin{cases} -\infty & if\ P_{in} \in (-\infty, P_{low}) \\ P_1 - |T_{21}| & if\ P_{in} \in (P_{low}, P_{high}) \\ P_1 & if\ P_{in} \in (P_{high}, \infty) \end{cases};$$

$$P_{out\_3} = P_{in} - |T_{31}| = \begin{cases} P_1 & if\ P_{in} \in (-\infty, P_{low}) \\ P_1 - |T_{31}| & if\ P_{in} \in (P_{low}, P_{high}) \\ -\infty & if\ P_{in} \in (P_{high}, \infty) \end{cases} \quad (1)$$

- Mode II:

$$P_2 = P_{in};$$

$$P_{reflected\_2} = P_{in} - |\Gamma_2| = \begin{cases} P_2 & if\ P_{in} \in (-\infty, P_{low}) \\ P_2 - |\Gamma_2| & if\ P_{in} \in (P_{low}, P_{high}) \\ -\infty & if\ P_{in} \in (P_{high}, \infty) \end{cases}$$

$$P_{out\_1} = -\infty \forall P_{in};$$

$$P_{out\_3} = P_{in} - |T_{32}| = \begin{cases} -\infty & if\ P_{in} \in (-\infty, P_{low}) \\ P_2 - |T_{32}| & if\ P_{in} \in (P_{low}, P_{high}) \\ P_2 & if\ P_{in} \in (P_{high}, \infty) \end{cases} \quad (2)$$

- Mode III:

$$P_3 = P_{in};$$
$$P_{out\_1} = P_3 \forall P_{in};$$
$$P_{out\_2} = -\infty \forall P_{in}; \quad (3)$$

where P_1, P_2, P_3, P_{out_1}, P_{out_2}, P_{out_3}, $P_{reflected\_2}$, and P_{in} (dBm) are the power values flowing into ports 1 to 3, power flowing out at ports 1 to 3, power reflected at port 2, and power of the incident signal, respectively.

Based on (1) and (2), at state I-M for the medium power level between P_{low} and P_{high}, the signal flows out from both port 2 and port 3. In this case, the proposed network functions as a power divider with a controllable power output ratio P_{out_2}/P_{out_3} modulated by the input power level. Considering state II-M, the signal will partly flow from port 2 to port 3 and partly be reflected, as expressed by $P_{reflected\_2}$. Consequently, the ratio $P_{reflected\_2}/P_{out\_3}$ is also adjustable as in state I-M.

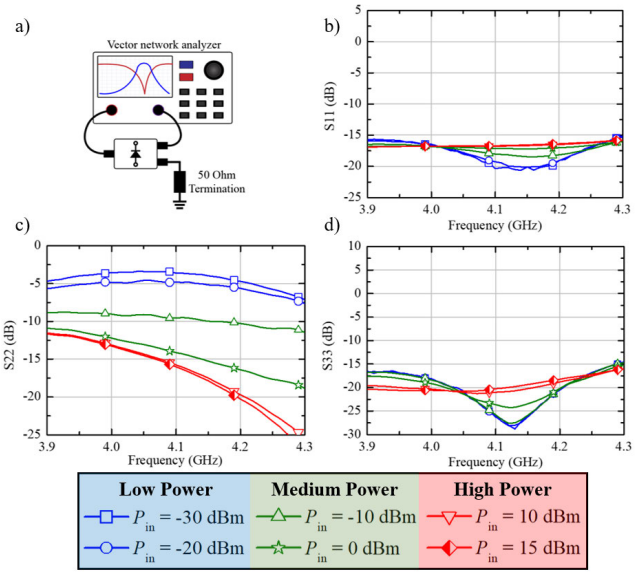

FIGURE 4. Experimental investigation of the proposed BSRM network. (a) Experimental configuration for measuring scattering parameters. (b)–(d) Reflection coefficients of the proposed network at different power levels, including three regions: low, medium, and high power.

As a proof of concept, the proposed network was designed and experimentally investigated at 4 GHz band with the thresholds P_{low} and P_{high} of -20 dBm and $+10$ dBm, respectively. Investigated prototype is constructed by incorporating previously mentioned power-dependent network with a circulator. The performance of the proposed BSRM network is measured with a Keysight N5227B PNA. Fig. 4(b)–(d) illustrate the measured reflection coefficient of each port at different power levels. The input power range is classified into three regimes, namely low, medium, and high. As can be observed, the measured reflection coefficients at port 1 and port 3 change only minimally with variation in the input power levels. Meanwhile, the measured reflection coefficients at port 2 vary significantly. Specifically, at 4.1 GHz,

the measured S_{22} decreases from −3.62 to −16.02 dB when the incident power level is varied from −30 to 15 dBm. This result is appropriate for the structure of the proposed network, as depicted in the equivalent circuit in Fig. 3. Owing to the existence of a power-dependent network in the connection between the circulator and port 2, this port has variable characteristics based on the input power. Meanwhile, the other ports are incapable of a similar functionality because the power-dependent network is not used with these ports.

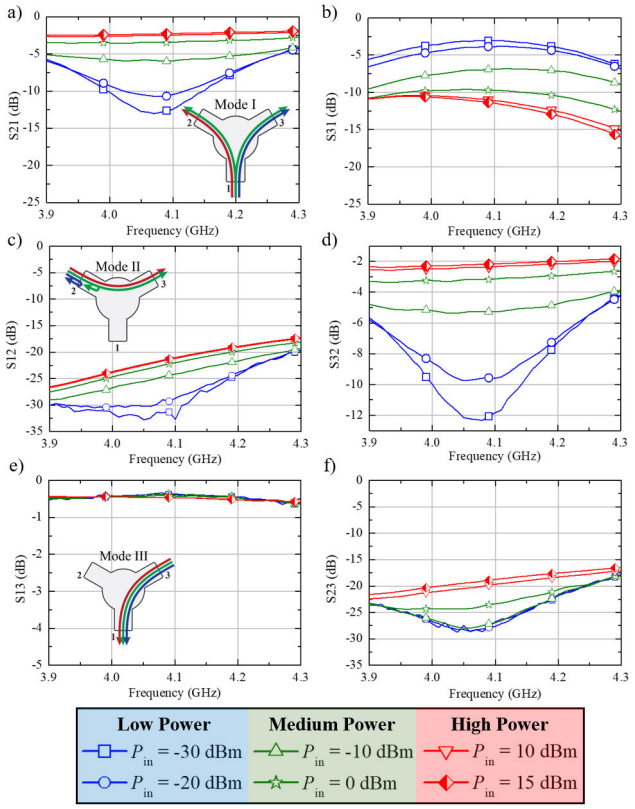

FIGURE 5. Measured transmission coefficient at different power levels: Insertion loss and isolation of the proposed structure at (a, b) Mode I; (c, d) Mode II; and (e, f) Mode III.

The remaining scattering parameters are concurrently considered, as depicted in Fig. 5. As previously discussed, the transmission coefficients of signals flowing from ports 1 to 3, ports 1 to 2, and ports 2 to 3 closely depend on variations in input power. Specifically, at 4.1 GHz, the measured insertion loss S_{21} significantly changes from −12.45 to −2.26 dB with variation in the incident power level from −30 to 15 dBm. In addition, S_{31} and S_{32} vary from −3.04 to −11.46 dB and −11.84 to −2.16 dB, respectively. The measured results have confirmed the operation of the proposed structure.

To achieve a better observation on the proposed BSRM network operation, the resulting powers at 4.1 GHz of mode I, II, and III for P_{in} of −30–15 dBm are extracted from the measured scattering parameters and presented in Fig. 6(b)–(d). Specifically, at Mode I with low P_{in}, P_{out_3} is 9.5 dB higher than P_{out_2} (for $P_{in} = -30$ dBm), indicating that most of the RF power flows out at port 3. The difference between P_{out_2} and P_{out_3} decreases and reaches a balanced value if P_{in} is increased to the medium power level. Above the balance point, P_{out_2} is more dominant than P_{out_3} with a difference of 9.3 dB at $P_{in} = 15$ dBm if P_{in} continues increasing, which indicates that the majority of the RF signal at high power flows out at port 2. A similar trend is observed at Mode II with P_{out_3} and $P_{reflected\_2}$ (Fig. 6(c)). A low P_{in} RF signal is mostly reflected at port 2, which is expressed as an 8.2 dB higher $P_{reflected\_2}$ compared to P_{out_3} at $P_{in} = -30$ dBm. Meanwhile, $P_{reflected\_2}$ is negligible under a high P_{in} RF signal, and the majority of the RF signal flows out at port 3, which is seen as a 13.9 dB higher P_{out_3} compared to $P_{reflected\_2}$ at $P_{in} = 15$ dBm. The balance point between $P_{reflected\_2}$ and P_{out_3} is observed in the medium range of P_{in}. At Mode III, the level of P_{in} does not affect the RF signal flow (Fig. 6(d)). In general, the experimental results convincingly validate the aforementioned operation of the proposed BSRM network.

The steps of design method for a BSRM network can be briefly summarized as follows:

1. Diode characterization to find out the equivalent values of L_s, C_p, and R_p with different power levels.
2. Power-dependent network design based on impedance matching at a specific power level and mismatching at other levels.
3. Incorporating designed network with passive static navigators to achieve desire operations.

TABLE 2. Operation summary of the proposed BSRM network at different power levels.

Mode	Low power	Medium power	High power
I	Through from port 1-3	Power divider with tuneable P_2/P_3	Through from port 1-2
II	Reflector	Power divider with tuneable P_2'/P_3	Through from port 2-3
III	Through from port 3-1	Through from port 3-1	Through from port 3-1

In conclusion, a BSRM network that is controlled via RF power level and completely independent of supporting electronic devices or components can thus be achieved using variations in the diode impedances at different power levels and by incorporating a passive navigator. Owing to passive manipulation using the changes in the incident RF signal power levels, the proposed network achieves a dynamically self-reconfigurable operation with three states for each mode, as summarised in Table 2. Owing to the main features of a controllable output power ratio and signal flow, the most suitable applications would be the one whose performances are strongly related to power ratio of different channels, such as polarization reconfigurable antennas, beam-steering, beam-reconfigurable antenna arrays, or even further applied in amplitude modulation RF schematic. Despite of the

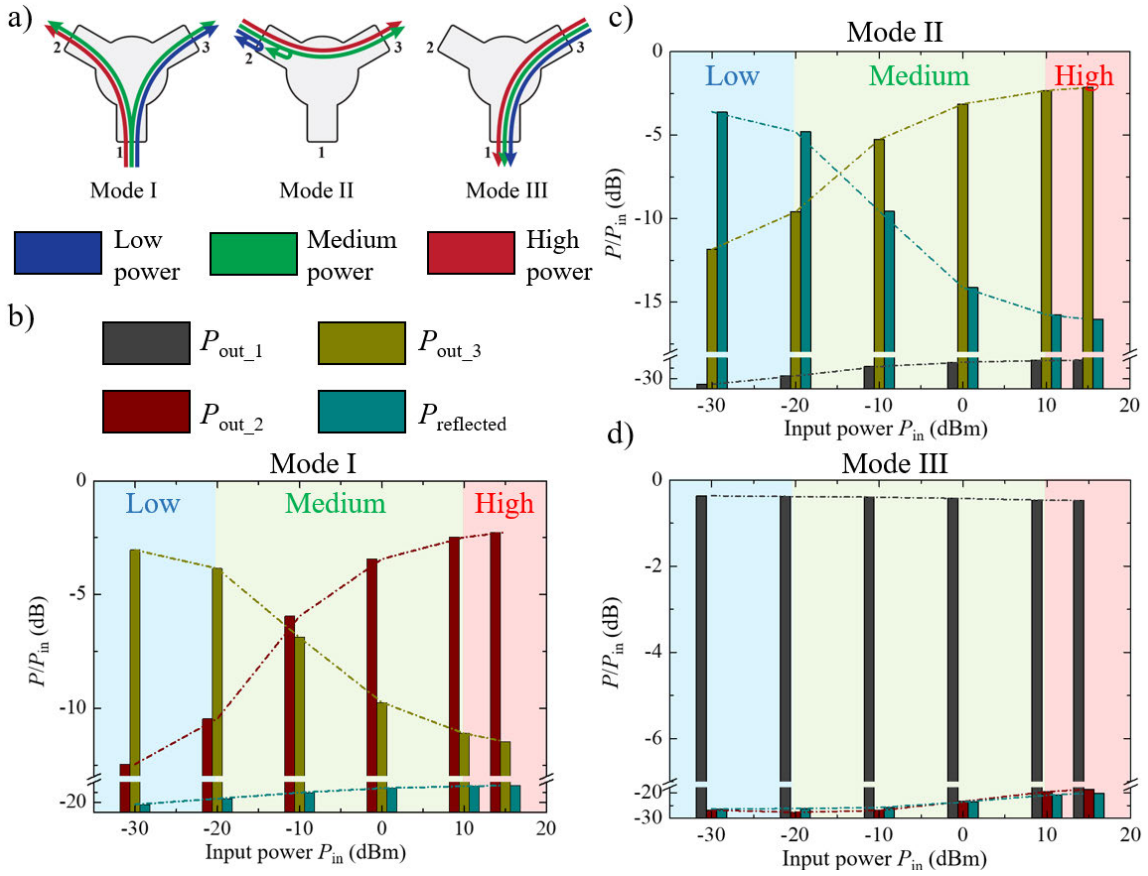

FIGURE 6. Experimental investigation of the proposed BSRM network. (a) Operational illustration of the proposed structure for different modes and power levels. (b)–(d) Resulting powers of the proposed structure at Modes I, II, and III for different input power levels.

differences in initial design purposes, the proposed network also can used as a half-duplex SPDT to navigate the signals. In this scenario, the ideal mode is mode I. To avoid the consequences of leakage power toward the configuration that is not the best suited, the isolation between 2 channels should be at least 10 dB. Therefore, the best option is using two well-separated power levels which are totally in high or low power range. For the case of proposed BSRM network, the suitable power levels should be bigger than 15 dBm or lower than −30 dBm to achieve that acceptable isolation. To achieve better performance as a half-duplex SPDT, the proposed principle could be extended with more complicated power-dependent network which use multiple diodes or different matching topologies to increase the difference between the impedance of each power levels. As such, the isolation between different ports of designed network can be significantly enhanced. In addition, a more sensitive BSRM network with minimal power range for the reconfiguration can also be achieved by using the same method. However, in this proposed work, a wide power range from −30 dBm to 20 dBm is necessary to separate transmitting power and receiving power due to the fact that the receiving power is conventionally much less than −30 dBm whereas 20 dBm is typical transmitting power.

C. PURELY SELF-POLARISATION-RECONFIGURABLE (PSPR) ANTENNA

The function of a reconfigurable antenna can typically be switched using an external controller. However, when a two-port antenna is combined with the proposed BSRM network, its characteristics can be self-switched without any external electronic devices, such as a DC bias network or digital control via microcontroller. As a demonstration, a dual-feed microstrip patch antenna was built on a 1.2 mm thick FR4 substrate with a dielectric constant of $\varepsilon = 4.1$ and loss tangent of $\delta = 0.02$. The power-dependent portion of the BSRM network was constructed at port 1 of the antenna with a Schottky diode SMS7630, as demonstrated in Fig. 7(a). Consequently, port 1 of the proposed structure functioned as a power-dependent port, and the static navigator portion was handled by an external circulator. The polarisation was handled by a patch antenna with two perpendicular ports (Fig. 7(b)). Such a configuration is similar to the case in which ports 2 and 3 of the proposed BSRM network are

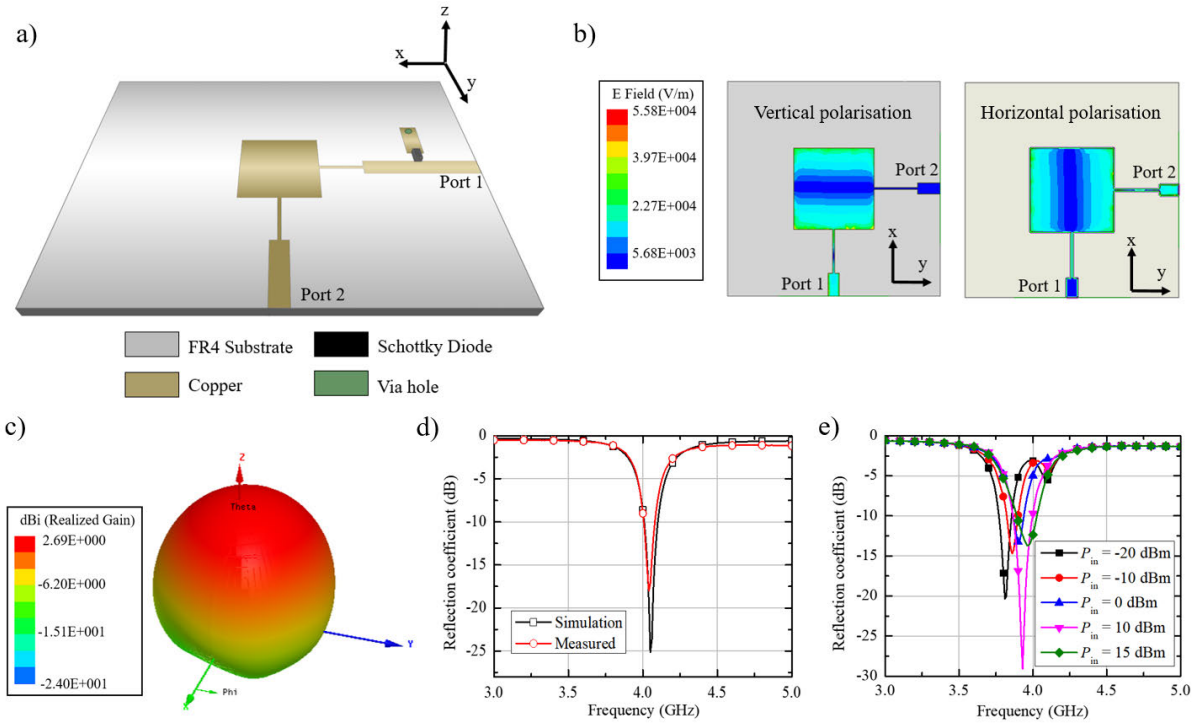

FIGURE 7. Proposed purely self-polarisation-reconfigurable (PSPR) antenna. (a) Perspective view of the proposed structure. (b) Electric field distributions of the patch antenna for different feeding positions. (c) Simulated 3D radiation pattern of the dual-feed patch antenna at 4.1 GHz. (d) Simulated and measured reflection coefficients of the dual-feed patch antenna (without the proposed power-dependent network). (e) Measured reflection coefficients of the proposed structure for the power-dependent port (port 1) at different power levels.

connected to ports 1 and 2 of the patch radiated portion, respectively.

The simulated electric field distribution for each feeding position is depicted in Fig. 7(b). If the radiating patch is fed using port 1, the radiated electromagnetic (EM) wave has vertical polarisation (VP). Otherwise, it has horizontal polarisation (HP) if the radiating patch is fed using port 2. Fig. 7(c) presents the simulated 3D radiation patterns of the designed structure at 4.1 GHz. A full-wave analysis reveals that the designed patch antenna without the power-dependent network achieves a 10 dB impedance bandwidth in the range of 4.01–4.10 GHz, with a peak gain of 2.69 dBi at 4.1 GHz. The simulated and measured reflection coefficients of the designed patch antenna are in good agreement, as depicted in Fig. 7(d). In contrast, the measured reflection coefficients of the designed patch antenna with a power-dependent network at different power levels are presented in Fig. 7(e). When the power varies from −20 dBm to 15 dBm, the measured return losses achieve a peak of 20.35 dB at 3.81 GHz for −20 dBm. With a signal level of 15 dBm, the highest return loss of 13.68 dB is observed at 3.97 GHz. These measured data confirm the close relationship of the proposed structure to the incident power level. To completely construct a PSPR antenna, a circulator is used for further measurements.

The geometry dimensions of the fabricated antenna are given in Fig. 8(a). Fig 8(b)–(e) provide parametric studies on the geometry dimensions of proposed PSPR antenna. As can be observed from Fig 8(b, c), the variations of patch length L and patch width W significantly affect to radiation performance of antenna. On the other hand, the variation on length L_{stub} of the shorted stub which connects the diode with ground plane would affect to the impedance matching performance of the proposed PSPR antenna, whereas the width W_{stub} of the shorted stub only shows a negligible effect, as shown in Fig. 8(d, e).

Because a dual-feed patch antenna is incorporated with the proposed BSRM network, the signal flows in the proposed PSPR antenna will be divided into two separate paths based on the power levels. By directing these signal flows to the designed dual-feed antenna, the radiated waves can be being self-manipulated using the power levels of the input signals. Ports 2 and 3 of the proposed BSRM network are connected to ports 1 and 2 of the patch radiated portions, respectively. At low input power (less than -20 dBm), the BSRM network is in state I-L (see Table 2); therefore, the signal will flow into port 2 of the antenna, and the EM wave is radiated with HP. Meanwhile, when the power of the incident signal exceeds the high-power threshold of 10 dBm, the BSRM network is in state I-H, the designed dual-feed patch antenna generates a VP wave because the signal flows to port 1 of the antenna. In contrast, when the proposed antenna functions as a receiver, the BSRM network acts only in state III-L because of the low power of the incoming signal.

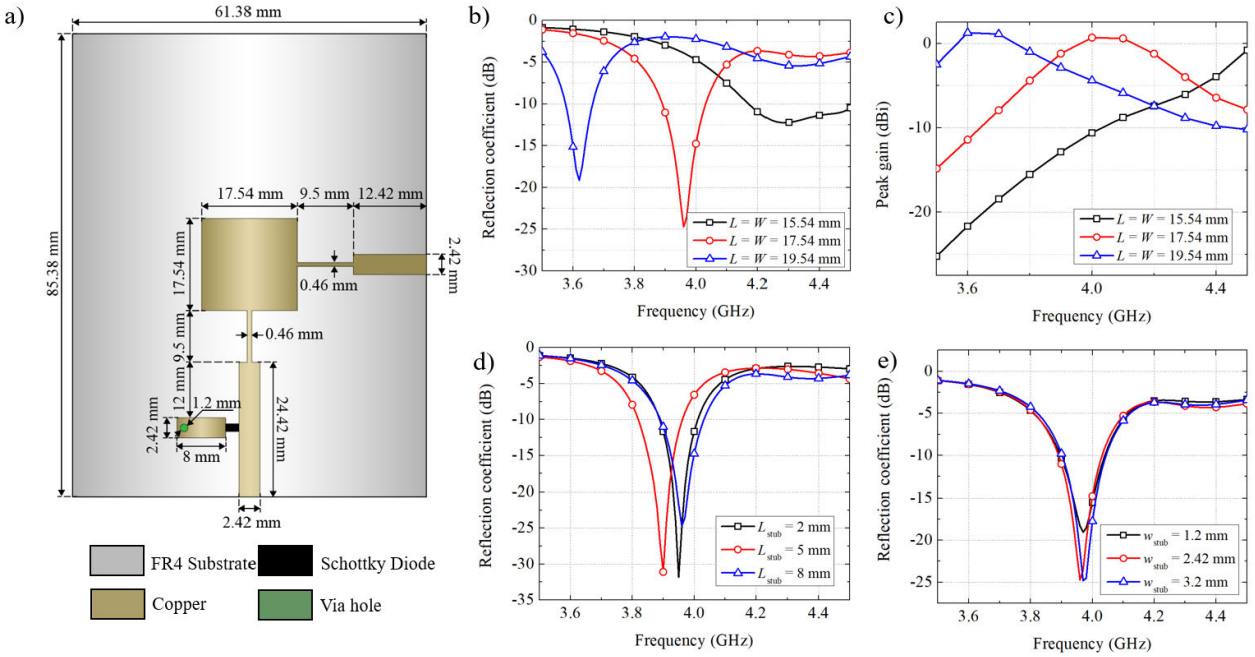

FIGURE 8. (a) Geometry dimensions of proposed PSPR antenna. (b, c) Simulated reflection coefficients and peak gain of proposed design with different patch antenna sizes. (d, e) Simulated reflection coefficients of proposed design with different size of shorted stub which connects diode with the ground plane.

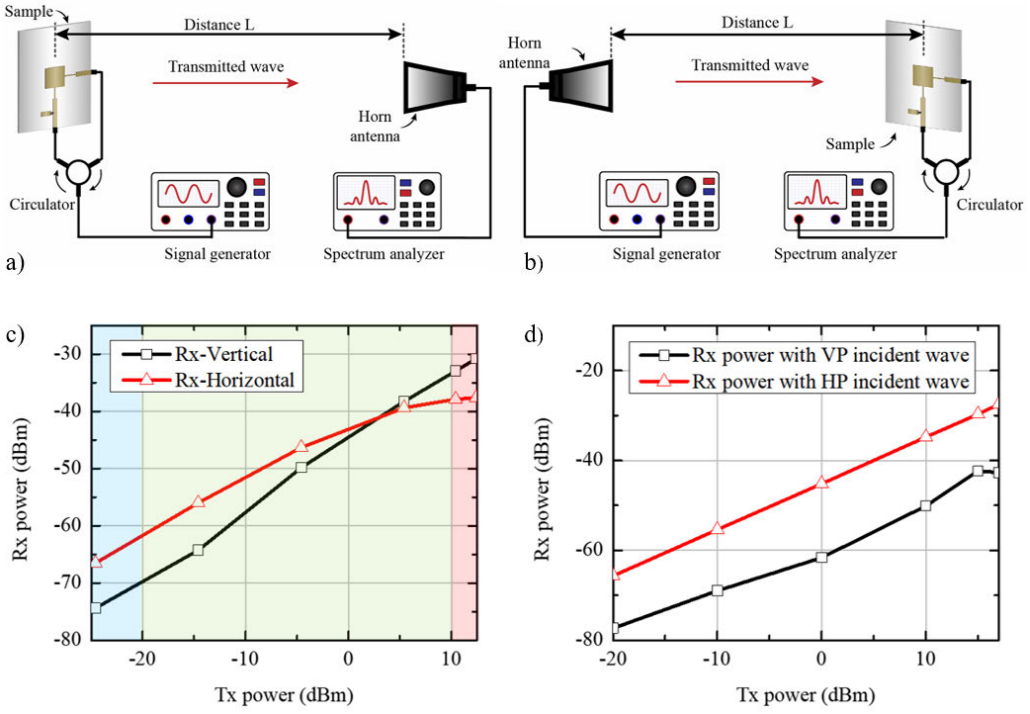

FIGURE 9. Experimental investigation of the proposed PSPR antenna. (a), (b) Configurations to investigate the operations of the proposed TX and RX antenna structures, respectively. (c), (d) Received power of the proposed structure with VP and HP EM waves, considered for the TX and RX states, respectively.

III. EXPERIMENTAL VERIFICATION

The self-polarisation-reconfiguration of the proposed PSPR antenna is experimentally investigated as depicted in Fig. 9(a) and 9(b). The measurements for the proposed structure are realised in two scenarios where the designed structure sequentially functions as a TX and RX antenna.

Further, for comparison, an SGH395 standard horn antenna manufactured by Microwave Vision Group is used and sequentially installed in the vertical and horizontal directions to create and track the VP and HP EM waves. The experiments were conducted using an Agilent N5182A vector signal generator and a HP 8593E spectrum analyser. Generated signals have a central frequency of 4.01 GHz with a transmission distance of $L = 4.1$ m. The experimental results illustrate a close agreement with the theoretically expected behaviours and the operational mechanism of the proposed PSPR antenna.

Fig. 9(c) illustrates the measured received power of the VP and HP horn antennas when the proposed structure functions as a TX antenna. For the same generated TX power in the low-power range (less than -20 dBm) and same distance between the TX and RX antennas, the received power of the HP horn antenna is higher than that of the VP antenna, with a difference of approximately 10 dB. This result indicates that the proposed structure functions as a HP antenna in the low-power range. With the increment of the input TX power, the difference between the HP and VP received powers decreases. The HP and VP received powers achieve balance near 3 dBm of input TX power. When the input TX power continues increasing and exceeds the high-power threshold of 10 dBm, the VP received power becomes higher than the HP received power. This result indicates that the proposed structure functions as a VP antenna in the high-power range. Because the maximum generated power from our signal generator is 17 dBm and the cable loss is 4.6 dB, measurements for TX power exceeding 12.4 dBm are not available.

When the proposed structure functions as an RX antenna, the standard horn antenna is sequentially installed as a TX antenna with vertical and horizontal directions to generate the respective polarisations of the EM wave. Because of the free-space path loss, the received power is less than -20 dBm. Consequently, this value of the received power maintains the proposed structure under its low-power state. As illustrated in Fig. 9(d), the measured received power of the proposed antenna exhibited a difference between the incoming HP and VP EM wave. The HP received power remained higher than the VP received power, with the highest difference of 16.41 dB at -61.6 dBm of received power. This result confirms that for low incident RF power, the proposed structure only functions as a HP antenna.

IV. CONCLUSION

We proposed a concept, strategy, and design for a novel all-passive batteryless self-reconfigurable multimode network to control the RF signal flow and ratio dynamically and automatically by manipulating only the power level of the incident signal without any additional supporting electronic components. Thanks to the power-dependence which is created by all-passively smart-sensing the power level, the dependence of the device on sensing electronic circuits is completely eliminated. The proposed network was theoretically and experimentally investigated to validate the operational mechanisms. Our proposed strategy is primarily based on ingeniously exploiting the characteristics of nonlinear devices at different power levels to create impedance matching/mismatching states and integrating with nonreciprocal components. Consequently, the proposed network eliminates dependence on supporting electronic devices and achieves a highly flexible, all-passive, and dynamically self-controllable ability to manipulate RF signal flow and ratio with seven different sub-states corresponding to three input power level regimes. In the comparison with conventional actively controlling components which are typically used in RF systems, the proposed idea of a batteryless self-reconfigurable multimode network would bring considerable advantages to RF system, such as reducing the number of controlling signals, reducing the total consumed power, reducing the number of active components, and significantly simplifying the total design of an RF system.

By incorporating the proposed network in a dual-feed antenna, we demonstrated the applicability of the proposed structure in the design of the PSPR antenna, which can self-switch the polarisation between vertical and horizontal based on the input RF power level without any external electronic devices. The proposed idea is considerably useful when the difference in transmitting and receiving modes is necessary. For instance, proposed PSPR antenna can be applied to a polarisation encoding RFID chipless systems which would significantly enhance the coding efficiency owing to the polarisation diversity [57]. Instead of using complex reader systems with several antennas for transmitting/receiving or for different polarisations, using only one proposed PSPR antenna might be enough. Furthermore, since the proposed antenna is purely self-reconfigurable, there are completely no controlling, sensing, or DC power supplying components. Another application is backscatter-based communication system, in which the system needs to operate with different transmitting and receiving antennas [58]. In addition, the proposed idea can also be applied into electronic warfare system by incorporating with conventional methods of frequency hopping or spread spectrum. For examples, after processing with conventional methods, the transmitted signal be further periodically or randomly change its polarization following a pre-defined rules. By combining this technique with conventional mentioned methods, the levels of security can be considerably enhanced.

On the other hand, the proposed BSRM network can be extended to other radiating structures to achieve purely self-frequency and purely self-pattern reconfigurable antennas. The proposed scheme has the advantages of a unique, simple, and flexible structure compared with other reconfigurable techniques. Furthermore, the proposed BSRM is applicable not only to chipless purely self-reconfigurable antennas but also to other RF devices and systems.

In conclusion, the proposed work reveals a potential strategy for replacing traditional energy harvesters in RF networks for dynamically controlling RF signal flows and ratios without additional electronic components; this is expected to pave

a new path for purely self-reconfigurable or self-adaptive RF devices. With the proposed strategy, the field of reconfigurable devices and systems is now extendable and establishing an important milestone for the future development of smart RF devices. The application of the proposed work is not only limited to antennas but also might be extendable to other RF self-adaptive devices, such as RF filters, switches, and phase shifters, and so on.

REFERENCES

[1] W. B. Carlson, "Technology: Revolutionary of radio," *Nature*, vol. 535, no. 7612, p. 354, Jul. 2016.

[2] J. E. Brittain, "Electrical engineering Hall of fame: Guglielmo marconi," *Proc. IEEE*, vol. 92, no. 9, pp. 1501–1504, Aug. 2004.

[3] A. A. Abidi, "Direct-conversion radio transceivers for digital communications," *IEEE J. Solid-State Circuits*, vol. 30, no. 12, pp. 1399–1410, Dec. 1995.

[4] B. Razavi, "Design considerations for direct-conversion receivers," *IEEE Trans. Circuits Syst. II. Analog Digit. Signal Process.*, vol. 44, no. 6, pp. 428–435, Jun. 1997.

[5] A. Sabharwal, P. Schniter, D. Guo, D. W. Bliss, S. Rangarajan, and R. Wichman, "In-band full-duplex wireless: Challenges and opportunities," *IEEE J. Sel. Areas Commun.*, vol. 32, no. 9, pp. 1637–1652, Sep. 2014.

[6] J. Ma, N. J. Karl, S. Bretin, G. Ducournau, and D. M. Mittleman, "Frequency-division multiplexer and demultiplexer for terahertz wireless links," *Nature Commun.*, vol. 8, no. 1, Sep. 2017.

[7] E. G. Larsson, O. Edfors, F. Tufvesson, and T. L. Marzetta, "Massive MIMO for next generation wireless systems," *IEEE Commun. Mag.*, vol. 52, no. 2, pp. 186–195, Feb. 2014.

[8] T. K. Nguyen, H. H. Nguyen, and H. D. Tuan, "Max-min QoS power control in generalized cell-free massive MIMO-NOMA with optimal backhaul combining," *IEEE Trans. Veh. Technol.*, vol. 69, no. 10, pp. 10949–10964, Oct. 2020.

[9] T. Chi, S. Li, J. S. Park, and H. Wang, "A multifeed antenna for high-efficiency on-antenna power combining," *IEEE Trans. Antennas Propag.*, vol. 65, no. 12, pp. 6937–6951, Dec. 2017.

[10] W. Duan, X. Y. Zhang, S. Liao, K. X. Wang, and Q. Xue, "Multiport power combining patch antenna with stable reflection coefficient and radiation pattern in six polarization states," *IEEE Trans. Antennas Propag.*, vol. 67, no. 2, pp. 719–729, Feb. 2019.

[11] G.-L. Tan, R. E. Mihailovich, J. B. Hacker, J. F. DeNatale, and G. M. Rebeiz, "Low-loss 2- and 4-bit TTD MEMS phase shifters based on SP4T switches," *IEEE Trans. Microw. Theory Techn.*, vol. 51, no. 1, pp. 297–304, Jan. 2003.

[12] S. Gong, H. Shen, and N. S. Barker, "A 60-GHz 2-bit switched-line phase shifter using SP4T RF-MEMS switches," *IEEE Trans. Microw. Theory Techn.*, vol. 59, no. 4, pp. 894–900, Apr. 2011.

[13] L. Zhang, X. Chen, R. Shao, J. Dai, Q. Cheng, G. Castaldi, V. Galdi, and T. J. Cui, "Breaking reciprocity with space-time-coding digital metasurfaces," *Adv. Mater.*, vol. 31, no. 41, 2019, Art. no. 1904069.

[14] Z. Luo, Q. Wang, X. Zhang, J. Wu, J. Dai, L. Zhang, H. Wu, H. Zhang, H. Ma, Q. Cheng, and T. Cui, "Intensity-dependent metasurface with digitally reconfigurable distribution of nonlinearity," *Adv. Opt. Mater.*, vol. 7, no. 19, 2019, Art. no. 1900792.

[15] C. Huang, C. Zhang, J. Yang, B. Sun, B. Zhao, and X. Luo, "Reconfigurable metasurface for multifunctional control of electromagnetic waves," *Adv. Opt. Mater.*, vol. 5, no. 22, Nov. 2017, Art. no. 1700485.

[16] C. P. Scarborough, D. H. Werner, and D. E. Wolfe, "Functionalized metamaterials enable frequency and polarization agility in a miniaturized lightweight antenna package," *Adv. Electron. Mater.*, vol. 2, no. 2, Feb. 2016, Art. no. 1500295.

[17] H. W. Ott, *Electromagnetic Compatibility Engineering*. Hoboken, NJ, USA: Wiley, 2009.

[18] W. A. Radasky, C. E. Baum, and M. W. Wik, "Introduction to the special issue on high-power electromagnetics (HPEM) and intentional electromagnetic interference (IEMI)," *IEEE Trans. Electromagn. Compat.*, vol. 46, no. 3, pp. 314–321, Aug. 2004.

[19] S. Dang, O. Amin, B. Shihada, and M.-S. Alouini, "What should 6G be?" *Nature Electron.*, vol. 3, no. 1, pp. 20–29, Jan. 2020.

[20] R. T. Derryberry, S. D. Gray, D. M. Ionescu, G. Mandyam, and B. Raghothaman, "Transmit diversity in 3G CDMA systems," *IEEE Commun. Mag.*, vol. 40, no. 4, pp. 68–75, Apr. 2002.

[21] B.-J. Liu, J.-H. Qiu, C.-H. Wang, W. Li, and G.-Q. Li, "Polarization-reconfigurable cylindrical dielectric resonator antenna excited by dual probe with tunable feed network," *IEEE Access*, vol. 7, pp. 60111–60119, 2019.

[22] J.-S. Row and M.-J. Hou, "Design of polarization diversity patch antenna based on a compact reconfigurable feeding network," *IEEE Trans. Antennas Propag.*, vol. 62, no. 10, pp. 5349–5352, Oct. 2014.

[23] L.-Y. Ji, P.-Y. Qin, Y. J. Guo, C. Ding, G. Fu, and S.-X. Gong, "A wideband polarization reconfigurable antenna with partially reflective surface," *IEEE Trans. Antennas Propag.*, vol. 64, no. 10, pp. 4534–4538, Oct. 2016.

[24] M. K. Ishfaq, T. Abd Rahman, M. Himdi, H. T. Chattha, Y. Saleem, B. A. Khawaja, and F. Masud, "Compact four-element phased antenna array for 5G applications," *IEEE Access*, vol. 7, pp. 161103–161111, 2019.

[25] Y. Liu, Q. Cheng, A. N. Khan, H. Giddens, M. M. Torrico, and Y. Hao, "Low-profile beam steerable patch array with SIW feeding network," *IEEE Access*, vol. 8, pp. 164178–164186, 2020.

[26] D. Parker and D. C. Zimmermann, "Phased arrays—Part 1: Theory and architectures," *IEEE Trans. Microw. Theory Techn.*, vol. 50, no. 3, pp. 678–687, Mar. 2002.

[27] D. Parker and D. C. Zimmermann, "Phased arrays—Part II: Implementations, applications, and future trends," *IEEE Trans. Microw. Theory Techn.*, vol. 50, no. 3, pp. 688–698, Mar. 2002.

[28] C. E. Fay and R. L. Comstock, "Operation of the ferrite junction circulator," *IEEE Trans. Microw. Theory Techn.*, vol. MTT-13, no. 1, pp. 15–27, Jan. 1965.

[29] Y. Konishi, "Lumped element y circulator," *IEEE Trans. Microw. Theory Techn.*, vol. MTT-13, no. 6, pp. 852–864, Nov. 1965.

[30] M. Thomaschewski, V. A. Zenin, C. Wolff, and S. I. Bozhevolnyi, "Plasmonic monolithic lithium niobate directional coupler switches," *Nature Commun.*, vol. 11, no. 1, Feb. 2020, Art. no. 748.

[31] C. Caloz, A. Sanada, and T. Itoh, "A novel composite right-/left-handed coupled-line directional coupler with arbitrary coupling level and broad bandwidth," *IEEE Trans. Microw. Theory Techn.*, vol. 52, no. 3, pp. 980–992, Mar. 2004.

[32] M. J. Schindler and A. Morris, "DC-40 GHz and 20-40 GHz MMIC sPDT switches," *IEEE Trans. Microw. Theory Techn.*, vol. MTT-35, no. 12, pp. 1486–1493, Dec. 1987.

[33] C. Tinella, J. M. Fournier, D. Belot, and V. Knopik, "A high-performance CMOS-SOI antenna switch for the 2.5-5-GHz band," *IEEE J. Solid-State Circuits*, vol. 38, no. 7, pp. 1279–1283, Jul. 2003.

[34] S. Dey and S. K. Koul, "Reliability analysis of Ku-band 5-bit phase shifters using MEMS SP4T and SPDT switches," *IEEE Trans. Microw. Theory Techn.*, vol. 63, no. 12, pp. 3997–4012, Dec. 2015.

[35] B. Yu, K. Ma, F. Meng, K. S. Yeo, P. Shyam, S. Zhang, and P. R. Verma, "DC-30 GHz DPDT switch matrix design in high resistivity trap-rich SOI," *IEEE Trans. Electron Devices*, vol. 64, no. 9, pp. 3548–3554, Sep. 2017.

[36] M. Kim, E. Pallecchi, R. Ge, X. Wu, G. Ducournau, J. C. Lee, H. Happy, and D. Akinwande, "Analogue switches made from boron nitride monolayers for application in 5G and terahertz communication systems," *Nat. Electron.*, vol. 3, pp. 479–485, May 2020.

[37] Q. Pei-Yuan, A. R. Weily, Y. J. Guo, T. S. Bird, and L. Chang-Hong, "Frequency reconfigurable quasi-Yagi folded dipole antenna," *IEEE Trans. Antennas Propag.*, vol. 58, no. 8, pp. 2742–2747, May 2010.

[38] I. Lim and S. Lim, "Monopole-like and boresight pattern reconfigurable antenna," *IEEE Trans. Antennas Propag.*, vol. 61, no. 12, pp. 5854–5859, Dec. 2013.

[39] I. Lim, T. Yun, and S. Lim, "Low-profile pattern-reconfigurable antenna with vertical and horizontal shorting lines in grounded CPW technology," *IEEE IEEE Antennas Wireless Propag. Lett.*, vol. 13, pp. 1589–1592, 2014.

[40] Y. Tawk, J. Costantine, and C. G. Christodoulou, "An eight-element reconfigurable diversity dipole system," *IEEE Trans. Antennas Propag.*, vol. 66, no. 2, pp. 572–581, Feb. 2018.

[41] S. Tanaka, N. Shimomura, and K. Ohtake, "Active circulators—The realization of circulators using transistors," *Proc. IEEE*, vol. 53, no. 3, pp. 260–267, Mar. 1965.

[42] A. Li, S. Kim, Y. Luo, Y. Li, J. Long, and D. F. Sievenpiper, "High-power transistor-based tunable and switchable metasurface absorber," *IEEE Trans. Microw. Theory Techn.*, vol. 65, no. 8, pp. 2810–2818, Aug. 2017.

[43] Y. Li and A. Abbosh, "Electronically controlled phasing element for single-layer reconfigurable reflectarray," *IEEE Antennas Wireless Propag. Lett.*, vol. 11, no. 5, pp. 628–631, Jun. 2012.
[44] G. M. Rebeiz and J. B. Muldavin, "RF MEMS switches and switch circuits," *IEEE Microw. Mag.*, vol. 2, no. 4, pp. 59–71, Dec. 2001.
[45] T. J. Jung, I. J. Hyeon, C. W. Baek, and S. Lim, "Circular/linear polarization reconfigurable antenna on simplified RF-MEMS packaging platform in K-band," *IEEE Trans. Antennas Propag.*, vol. 60, no. 11, pp. 5039–5045, Nov. 2012.
[46] H. Wakatsuchi, S. Kim, J. J. Rushton, and D. F. Sievenpiper, "Waveform-dependent absorbing metasurfaces," *Phys. Rev. Lett.*, vol. 111, no. 24, Dec. 2013, Art. no. 245501.
[47] P. Nikitin, "Self-reconfigurable RFID reader antenna," in *Proc. IEEE Int. Conf. RFID (RFID)*, May 2017, pp. 88–95.
[48] Z. Luo, X. Chen, J. Long, R. Quarfoth, and D. Sievenpiper, "Nonlinear power-dependent impedance surface," *IEEE Trans. Antennas Propag.*, vol. 63, no. 4, pp. 1736–1745, Apr. 2015.
[49] R. Phon and S. Lim, "Dynamically self-reconfigurable multifunctional all-passive metasurface," *ACS Appl. Mater. Interface*, vol. 12, no. 37, pp. 42393–42402, Sep. 2020.
[50] J. Singh, R. Kaur, and D. Singh, "Energy harvesting in wireless sensor networks: A taxonomic survey," *Int. J. Energy Res.*, vol. 45, no. 1, pp. 118–140, Jan. 2021, doi: 10.1002/er5816.
[51] I. Ahmad, M. M. Rehman, M. Khan, A. Abbas, S. Ishfaq, and S. Malik, "Flow-based electromagnetic-type energy harvester using microplanar coil for IoT sensors application," *Int. J. Energy Res.*, vol. 43, no. 10, pp. 5384–5391, Aug. 2019.
[52] X. Wu and D. Lee, "Miniaturized piezoelectric energy harvester for battery-free portable electronics," *Int. J. Energy Res.*, vol. 43, no. 6, pp. 2402–2409, Mar. 2019.
[53] J. Siang, M. H. Lim, and M. S. Leong, "Review of vibration-based energy harvesting technology: Mechanism and architectural approach," *Int. J. Energy Res.*, vol. 42, no. 5, pp. 1866–1893, Apr. 2018.
[54] Y. Kim and S. Lim, "2.4-GHz high-efficiency rectenna using an in-phase partially reflective surface and high-order harmonic reject bandpass filter," *Electromagnetics*, vol. 34, no. 6, pp. 463–473, Aug. 2014.
[55] N. H. Nguyen, T. D. Bui, A. D. Le, A. D. Pham, T. T. Nguyen, Q. C. Nguyen, and M. T. Le, "A novel wideband circularly polarized antenna for RF energy harvesting in wireless sensor nodes," *Int. J. Antennas Propag.*, vol. 2018, Mar. 2018, Art. no. 1692018.
[56] D. A. Pham, E. Park, H. L. Lee, and S. Lim, "High gain and wideband metasurfaced magnetoelectric antenna for WiGig applications," *IEEE Trans. Antennas Propag.*, vol. 69, no. 2, pp. 1140–1145, Feb. 2021.
[57] A. Vena, E. Perret, and S. Tedjini, "A compact chipless RFID tag using polarization diversity for encoding and sensing," in *Proc. IEEE Int. Conf. RFID (RFID)*, Orlando, FL, USA, Apr. 2012, pp. 191–197.
[58] E. Denicke, H. Hartmann, N. Peitzmeier, and B. Geck, "Backscatter beamforming: A transponder for novel MIMO RFID transmission schemes," *IEEE J. Radio Freq. Identificat.*, vol. 2, no. 2, pp. 80–85, Jun. 2018.

DUC ANH PHAM was born in Stollberg, Germany, in 1994. He received the B.Eng. degree in electrical engineering from the Hanoi University of Science and Technology (HUST), Hanoi, Vietnam, in 2017, and the M.S. degree in microwave and optics from the School of Electrical and Electronics Engineering, Chung-Ang University (CAU), Seoul, South Korea, in 2020, where he is currently pursuing the Ph.D. degree.

From 2017 to 2018, he was an RF Engineer with Viettel Aerospace Institute, where he involved in researching and developing microwave circuits and systems for aerospace and defense industry. His research interests include millimeter-wave antennas, reconfigurable antennas, and metasurfaced antennas.

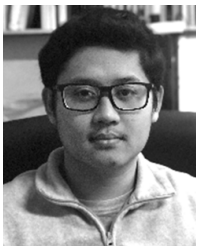

RATANAK PHON was born in Kandal, Cambodia, in 1994. He received the B.S. degree in electrical and electronics from the Institute of Technology of Cambodia, Phnom Penh, Cambodia, in 2017. He is currently pursuing the M.S. and Ph.D. degrees in an integrated program with the School of Electrical and Electronics Engineering, Chung-Ang University, Seoul, South Korea. His current research interests include metamaterials, frequency selective surfaces, and reconfigurable structures.

YEONJU KIM received the B.S. and M.S. degrees from the School of Electrical and Electronics Engineering, Chung-Ang University, Seoul, South Korea, in 2012 and 2014, respectively, where she is currently pursuing the Ph.D. degree in electrical and electronics engineering. Her research interests include design and analysis of microwave and millimeter wave antennas, and 3D printed RF electronics.

SUNGJOON LIM (Member, IEEE) received the B.S. degree in electronic engineering from Yonsei University, Seoul, South Korea, in 2002, and the M.S. and Ph.D. degrees in electrical engineering from the University of California at Los Angeles (UCLA), Los Angeles, CA, USA, in 2004 and 2006, respectively.

After a postdoctoral position at the Integrated Nanosystems Research Facility (INRF), University of California at Irvine, Irvine, CA, USA, he joined the School of Electrical and Electronics Engineering, Chung-Ang University, Seoul, in 2007, where he is currently a Professor. He has authored and coauthored more than 250 international conference, letter, and journal articles. His research interests include engineered electromagnetic structures, such as metamaterials, electromagnetic bandgap materials, and frequency selective surfaces, printed antennas, substrate integrated waveguide (SIW) components, inkjet-printed electronics, and RF MEMS applications. He is also interested in the modeling and design of microwave circuits and systems.

Dr. Lim received the Institution of Engineering and Technology (IET) Premium Award, in 2009, the ETRI Journal Best Paper Award, in 2014, the Best Paper Award from the 2015 International Workshop on Antenna Technology (iWAT) and the 2018 International Symposium on Antennas and Propagation (ISAP), and a CAU Distinguished Scholar, from 2014 to 2020.